Experimental and theoretical investigation of the triple differential cross section for electron impact ionization of pyrimidine molecules

J. D. Builth-Williams,[1] S. M. Bellm,[1,a)] D. B. Jones,[1] Hari Chaluvadi,[2] D. H. Madison,[2] C. G. Ning,[3] B. Lohmann,[4] and M. J. Brunger[1,5,a)]
[1]*ARC Centre of Excellence for Antimatter-Matter Studies, Flinders University, GPO Box 2100, Adelaide, South Australia 5001, Australia*
[2]*Department of Physics, Missouri University of Science and Technology, Rolla, Missouri 65409, USA*
[3]*Department of Physics and Key Laboratory of Atomic and Molecular NanoSciences of MOE, Tsinghua University, Beijing 100084, People's Republic of China*
[4]*University of the Sunshine Coast, Maroochydore DC, Queensland 4558, Australia*
[5]*Institute of Mathematical Sciences, University of Malaya, 50603 Kuala Lumpur, Malaysia*

(Received 14 November 2011; accepted 14 December 2011; published online 9 January 2012)

Cross-section data for electron impact induced ionization of bio-molecules are important for modelling the deposition of energy within a biological medium and for gaining knowledge of electron driven processes at the molecular level. Triply differential cross sections have been measured for the electron impact ionization of the outer valence $7b_2$ and $10a_1$ orbitals of pyrimidine, using the (e, 2e) technique. The measurements have been performed with coplanar asymmetric kinematics, at an incident electron energy of 250 eV and ejected electron energy of 20 eV, for scattered electron angles of -5°, -10°, and -15°. The ejected electron angular range encompasses both the binary and recoil peaks in the triple differential cross section. Corresponding theoretical calculations have been performed using the molecular 3-body distorted wave model and are in reasonably good agreement with the present experiment. © *2012 American Institute of Physics*. [doi:10.1063/1.3675167]

I. INTRODUCTION

Studies of the electron-impact ionization of bio-molecules provide important information on the role of electrons in causing damage to DNA in biological systems. It is now well established that low energy secondary electrons produced by high energy primary radiation are responsible for much of the damage to DNA in living tissue.[1,2] In order to predict cellular damage it is desirable to model the trajectories of primary and secondary particles through a biological medium. This can be done by calculating the path along which the primary and secondary particles move as they pass through matter, known as their charged particle track structures.[3–6] Detailed information is required on the initial spatial distribution of events involving both ionization and excitation along the charged particles path. Differential cross sections are an important source of this information as they enable a complete three-dimensional description of the deposition of energy as a function of angle.[5] In the majority of track structure simulations in biological media, the focus is on water[3,6] as the primary species in the system, but the inclusion of contributions from other species present is needed for a more complete description of the process. Due to the challenging nature of performing measurements and calculations of cross-sectional data for electron interactions with larger molecules, there are currently limited data for targets of biological interest.

Pyrimidine ($C_4H_4N_2$) is an important molecule of biological significance. It possesses a six membered ring structure belonging to the group of diazines, where the two nitrogen atoms in the ring are located in the meta positions. The molecular point group of pyrimidine is C_{2v}. The pyrimidine molecule is of particular interest because it forms the fundamental structure in several nucleobase ring systems, and it is because of this structural similarity that it has been used as a model compound to investigate electron collisions with DNA constituents.[7–9] Indeed, two of the four nucleobases found in DNA, that is cytosine and thymine, as well as the RNA base uracil are pyrimidine derivatives.

The power of the electron-electron coincidence (e, 2e) technique for investigating the ionization dynamics of atoms and molecules is well recognized.[10] In an (e, 2e) experiment information about the collision of an incident electron with an atomic or molecular target is obtained by measuring the energy and momenta of the outgoing electrons in time coincidence. The technique can be used to provide spatial information about the scattering direction of electrons. A key objective of the present study is to further our understanding of electron interactions with bio-molecules, using smaller molecules to compare directly with the components of larger biological systems. While measuring cross sections for isolated molecules in the gas phase can, of course, only approximate what occurs in biological systems, it is good starting point and has proven to be a useful approach.[11–13]

Despite the fact that many dynamical (e, 2e) studies of atomic systems have been reported, low-energy (e, 2e) studies of molecules have not been as numerous. Indeed, while there has been an increased interest in these studies over the last

a)Authors to whom correspondence should be addressed. Electronic addresses: susan.bellm@flinders.edu.au and michael.brunger@flinders.edu.au.

decade, both theoretical and experimental studies have mostly been limited to smaller targets. Recently, molecules including methane[14,15] and formic acid[16] have been investigated. Studies concerning larger molecules such as component molecules of DNA and RNA are rare, and include tetrahydrofuran[17] and theoretical studies on thymine.[18] Difficulties in the theoretical calculations arise from the fact that the orientation of the molecule is not commonly determined by experiment and an averaging over all molecular orientations must be incorporated into the theoretical approach. Furthermore, the theoretical approach must include a multicentred wave function. This is in contrast to the much simpler atomic cases where atoms have only a single scattering centre and spherically symmetric wave functions.[19]

While to the best of our knowledge the present study represents the first dynamical (e, 2e) investigation of pyrimidine, the bound electronic structure has previously been probed by electron momentum spectroscopy (EMS). Ning *et al.* have reported EMS measurements of the complete valence region of pyrimidine at incident electron energies of 600 eV and 1500 eV, and compared their measured results with Hartree-Fock and density functional theory (DFT) calculations.[20] Shojaei *et al.* have also recently reported an extensive theoretical study of its valence electronic structure, ionization spectrum, and electron momentum distributions.[21] The valence electronic structure of pyrimidine and a number of its halogenated derivatives have also recently been investigated using ultraviolet photoelectron spectroscopy and *ab inito* quantum chemical methods.[22]

II. EXPERIMENTAL DETAILS

The electron impact induced single ionization of a ground state pyrimidine molecule, $C_4H_4N_2$, can be described by

$$e^-(E_i, \mathbf{k}_i) + C_4H_4N_2 \rightarrow C_4H_4N_2^+ + e^-(E_a, \mathbf{k}_a) + e^-(E_b, \mathbf{k}_b), \quad (1)$$

where E_i, E_a, E_b and $\mathbf{k}_i$, $\mathbf{k}_a$, $\mathbf{k}_b$ are the kinetic energies and momenta of the incident, scattered, and ejected electrons, respectively.

The triple differential cross section (TDCS) is represented by

$$\frac{d^5\sigma}{d\Omega_a d\Omega_b dE_b}, \quad (2)$$

and it is a measure of the probability that after ionization of a target species by a projectile with energy E_i and momentum $\mathbf{k}_i$, two electrons will be produced with energies E_a and E_b, and momenta $\mathbf{k}_a$ and $\mathbf{k}_b$ into the solid angles Ω_a and Ω_b. The momentum transferred to the target is

$$\mathbf{K} = \mathbf{k}_i - \mathbf{k}_a. \quad (3)$$

In the present study, coplanar asymmetric measurements were performed using a conventional coincidence spectrometer. The experimental apparatus has previously been described in detail[17,23] and so only a brief overview will be given here.

An incident beam of electrons is produced by thermionic emission from a tungsten filament and is collimated and transported to the interaction region using five cylindrical electrostatic lens elements. The resulting incident electron beam energy resolution is approximately 0.5 eV. At the interaction region the electron beam crosses a molecular target beam. The target beam enters the interaction region through a 0.7 mm internal diameter stainless steel capillary. In the current configuration of the apparatus, the capillary and thus the target beam are oriented parallel to the scattering plane, which is defined by the momentum vectors of the incident and measured outgoing electrons.

The higher energy (scattered) and lower energy (ejected) outgoing electrons are both detected in separate hemispherical energy analysers, each comprising a 5-element electrostatic entrance lens system, hemispherical selector, and channel electron multiplier detector. (e, 2e) events are identified using standard coincidence timing procedures[24] from the relative arrival times of electrons at the two detectors and background events are subtracted using standard statistical methods. The two electron energy analysers are mounted on independently rotatable turntables concentric with the interaction region. In dynamical TDCS measurements, the scattered electron is detected at a fixed (small) forward angle with respect to the incident electron beam direction. Ejected electron angular distributions are measured by scanning the ejected electron energy analyser and detecting electrons at a number of different angles within the scattering plane. In the current measurements the coincidence energy resolution of the system is approximately 1.1 eV (FWHM), as determined from a measurement of the helium 1*s* binding energy peak.

Pyrimidine is a liquid at room temperature with sufficient vapour pressure at room temperature to perform our measurements. The pyrimidine sample 99% (Sigma-Aldrich, Australia) was treated with several freeze-pump-thaw cycles prior to use to remove absorbed gases. To prevent possible condensation of pyrimidine within the sample lines, which may contribute to instability in the rate of flow of the sample into the vacuum chamber, the sample lines, and vacuum chamber were heated to approximately 40 °C throughout the measurements.

III. THEORETICAL FRAMEWORK

The molecular 3-body distorted wave (M3DW) approximation has been presented in previous papers,[25–27] so that only a brief outline of the theory will be presented. The TDCS for the M3DW is given by

$$\frac{d^5\sigma}{d\Omega_a d\Omega_b dE_b} = \frac{1}{(2\pi)^5}\frac{k_a k_b}{k_i}|T|^2, \quad (4)$$

where $\vec{k}_i$, $\vec{k}_a$, and $\vec{k}_b$ are the wave vectors for the initial, scattered, and ejected electrons. The scattering amplitude is given by

$$T = \left\langle \chi_a^-(\vec{k}_a, \mathbf{r}_1)\chi_b^-(\vec{k}_b, \mathbf{r}_2)C_{scat-eject}\left(r_{12}^{ave}\right)\middle| V - U_i\middle|\phi_{DY}^{OA}(\mathbf{r}_2)\chi_i^+(\vec{k}_i, \mathbf{r}_1)\right\rangle, \quad (5)$$

where r_1 and r_2 are the coordinates of the incident and the bound electrons, χ_i, χ_a, and χ_b are the distorted waves for the incident, scattered, and ejected electrons, respectively, and $\phi_{DY}^{OA}(r_2)$ is the initial bound-state Dyson molecular orbital

averaged over all orientations. The molecular wave functions were calculated using DFT along with the standard hybrid B3LYP (Ref. 28) functional by means of the ADF 2007 (Amsterdam density functional) program[29] with the triple-zeta with two polarization functions Slater type basis set. For the $7b_2$ orbital, the average of the absolute value of the Dyson wave function is taken since the normal average is zero.[15] The factor $C_{scat-eject}(r_{12}^{ave})$ is the Ward-Macek average Coulomb-distortion factor between the two final state electrons,[30] V is the initial state interaction potential between the incident electron and the neutral molecule, and U_i is a spherically symmetric distorting potential which is used to calculate the initial-state distorted wave for the incident electron $\chi_i^+(\vec{k}_i, \mathbf{r}_1)$.

The Schrödinger equation for the incoming electron wave function is given by

$$\left(T + U_i - \frac{k_i^2}{2}\right)\chi_i^+(\overrightarrow{k_i}, r) = 0, \tag{6}$$

where T is the kinetic energy operator and the "+" superscript on $\chi_i^+(\vec{k}_i, \mathbf{r})$ indicates outgoing wave boundary conditions. The initial state distorting potential contains three components $U_i = U_s + U_E + U_{CP}$, where U_s contains the nuclear contribution plus a spherically symmetric approximation for the interaction between the projectile electron and the target electrons which is obtained from the quantum mechanical charge density of the target. U_E is the exchange potential of Furness and McCarthy (corrected for sign errors)[31] which approximates the effect of the continuum electron exchanging with the passive bound electrons in the molecule, and U_{CP} is the correlation-polarization potential of Perdew and Zunger.[32,33]

The final state for the system is approximated as a product of distorted waves for the two continuum electrons times the average Coulomb-distortion factor. The final state distorted waves are calculated as the initial state except that the final state spherically symmetric static distorting potential for the molecular ion is used for U_s.

IV. RESULTS AND DISCUSSION

Figure 1 shows the present binding energy spectrum for the outer valence region of pyrimidine. The incident and ejected electron energies were fixed at 250 eV and 20 eV, respectively, while the scattered electron energy was scanned across a range of energies. The detection angles for the scattered and ejected electrons were selected to be -15° and 70°, respectively. As noted earlier, the experimental coincidence energy resolution under the chosen conditions was estimated to be 1.1 eV FWHM, from the width of the helium 1s binding energy peak measured under the same kinematics. The binding energy spectrum has been fitted with a sum of eight Gaussian functions of a fixed width, which corresponds to the experimental coincidence energy resolution. Note that as our coincidence energy resolution is much larger than the natural widths of the various orbitals,[34–38] this is a reasonable approximation in this case.

The valence electronic structure of pyrimidine is relatively well characterised. Photoelectron spectra of pyrimidine have been recorded using synchrotron radiation,[34,39] as well as HeI (Refs. 35, 36, and 38) and HeII (Ref. 37) radiation. Table I shows the binding energy determined for each orbital, as well as the binding energies determined in previous EMS (Ref. 20) and photoelectron spectroscopy (PES) (Ref. 34) studies which are in good agreement with the present results. We note that to facilitate their study of β parameters in the PES study by Potts *et al.*, pyrimidine was assigned in the C_s point group rather than the C_{2v} group.[34] It should also be noted that although the C_{2v} point group was adopted, a different notation has been used to label the orbitals in some of the previous pyrimidine PES studies.[22,36] The highest occupied molecular orbital (HOMO) is the $7b_2$ orbital which has a binding energy of 9.8 eV. With our coincidence energy resolution this cannot be fully resolved from the next highest $2b_1$ orbital. Note that the $7b_2$ orbital of pyrimidine can be considered as being essentially a non-bonding orbital associated with the N atoms.[40] The largest peak in the

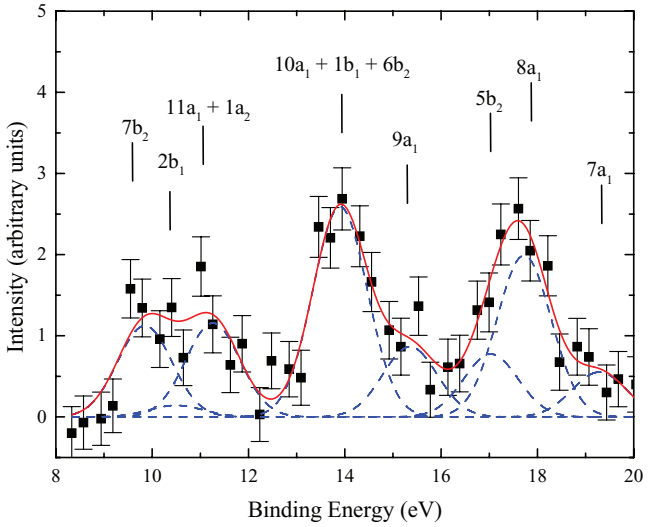

FIG. 1. Measured binding energy spectrum for the outer valence region of pyrimidine, obtained at an incident energy of 250 eV (see text for details). The data are fitted with a sum of Gaussian functions using the coincidence energy resolution as the peak width.

TABLE I. Binding energies for the outer valence region of pyrimidine in eV. The error in the Gaussian peak location for the present data is quoted in brackets. The orbital assignments, calculations, and EMS data are from Ning *et al.*[20] PES data are from Potts *et al.*[34]

Orbital	Type	Present results (eV)	PES (eV)[a]	EMS (eV)[b]	OVGF (eV)[a]
$7b_2$	nσ	9.8 (0.2)	9.8	9.8	9.83
$2b_1$	π	10.5 (0.6)	10.5	10.5	10.4
$11a_1$	nσ	11.3 (0.2)	11.2	11.3	11.36
$1a_2$	π		11.5		11.28
$10a_1$	σ	13.9 (0.1)	13.9	14.1	14.49
$1b_1$	π				14.49
$6b_2$	σ		14.4		14.63
$9a_1$	σ	15.4 (0.3)	15.8	15.7	16.25
$5b_2$	σ	17.0 (0.9)	17.0	17.5	17.26
$8a_1$	σ	17.7 (0.4)	17.7		18.28
$7a_1$		19.4 (0.2)		20.6	

[a]Reference 34.
[b]Reference 20.

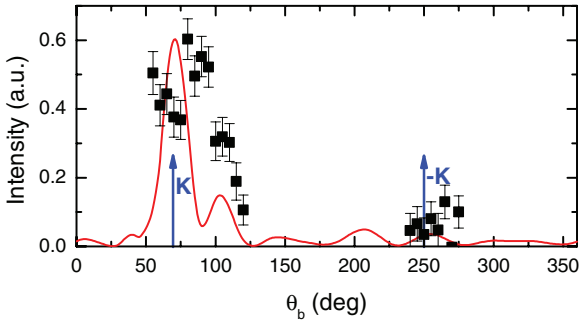

FIG. 2. Plot of the triple differential cross sections for ionization of the $7b_2$ orbital of pyrimidine, with $E_0 = 250$ eV and $E_b = 20$ eV. The scattered electron detection angle is -15° and the corresponding momentum transfer is $|K| = 1.12$ a.u. Points are the experimental data. Solid curve (red): M3DW calculation taking the average of the absolute value of the Dyson wave function. The positions of the momentum transfer vector, **K**, and $-$**K** are indicated by the arrows.

spectrum shown in Fig. 1, at a binding energy of 13.9 eV, is assigned as being predominantly due to ionization of the $10a_1$ orbital although contributions from the $1b_1$ and $6b_2$ orbitals are also likely to be present.

Experimental and theoretical TDCSs for the outermost $7b_2$ orbital of pyrimidine at a scattering angle of -15° are presented in Figure 2. The measurements were performed at a relatively low incident electron energy of 250 eV and the energy for the ejected electron was chosen to be 20 eV. As the energy separation between the HOMO and the next highest occupied molecular orbital is only 0.7 eV, well below the 1.1 eV FWHM coincidence resolution of our apparatus, we reiterate that the data in the present measurements most likely contains contributions from both orbitals. The uncertainties on the present $7b_2$ TDCS are statistical and are at the one standard deviation level.

Conventionally, the angular distributions are divided into two regions.[24] These are the angular region between 0° and 180°, which is known as the binary region, and the region between 180° and 360° which is named the recoil region. The binary region may contain strong signatures of the orbital structure whereas the recoil region contains structure arising from processes in which the ejected electron undergoes an initial binary collision and then subsequent elastic backscattering from the residual ion core. The present experimental $7b_2$ orbital binary peak data appears (see Fig. 2) to have a double peak type structure with a local minimum in the angular range very close to the momentum transfer direction. The slight shift of the binary peak, to larger scattering angles, away from the momentum transfer direction is likely caused by Coulomb repulsion between the final state electrons. A double peak type structure in the binary peak of atomic orbitals is characteristic of a *p*-type orbital and reflects the momentum probability density distribution of electrons in these orbitals.[41] The $7b_2$ orbital is of N $2p$ character,[34] thus the observed structure most likely reflects the $2p$ nature of the molecular orbital. The M3DW predicts a double binary peak as well but the peak positions are shifted to larger scattering angles by about 20° and the second peak has a much lower intensity than the experimental data.

The M3DW calculation also predicts the relative magnitudes of the $7b_2$ orbital binary and recoil peaks quite well. As the experimental data are relative they are only attributed absolute values by normalization to the M3DW theory to give the best visual fit in the binary peak region. The size of the recoil peak is small, indicating that there is not a large amount of interaction of the ejected electron with the molecular ion. This is expected as the kinematics are close to bound Bethe ridge conditions. On the Bethe ridge the kinematics satisfy the requirement that all momentum is transferred to the bound, target electron during the collision. Under such conditions, the collision kinematics correspond to a binary e–e collision, where the ion plays no role, and practically no recoil lobe is expected. Interestingly, the HOMO binary peak here also appears quite narrow. This is in contrast to previous dynamical (e, 2e) studies on molecules, including for tetrahydrofuran,[17] formic acid,[16] water,[42] nitrogen,[43] and methane,[14] under similar kinematics in which very broad binary peaks have been observed for ionization of the HOMO.

Triple differential cross sections for the $10a_1$ orbital of pyrimidine, at scattered electron angles of -5, -10°, and -15°, are shown in Figures 3(a)–3(c). These measurements were also performed at an incident electron energy of 250 eV and the energy of the ejected electron was 20 eV.

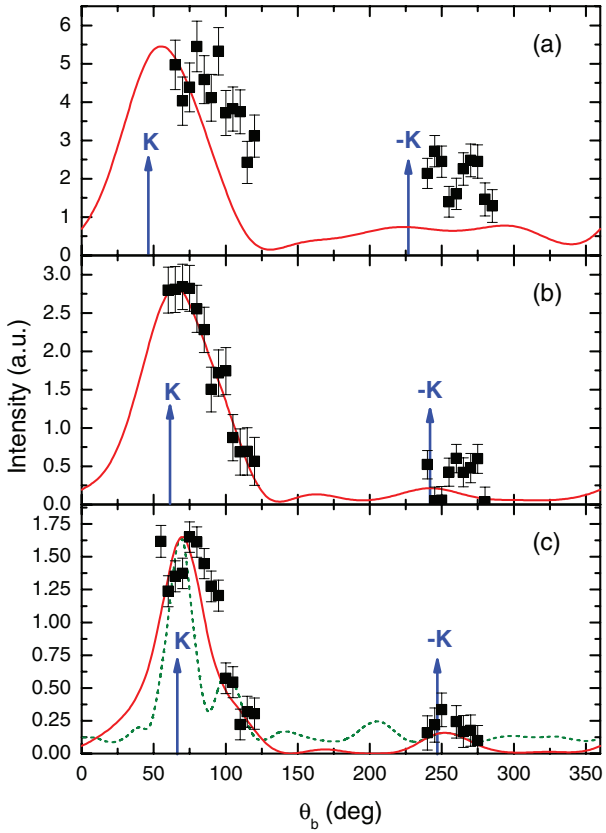

FIG. 3. Plot of the triple differential cross sections for ionization of the $10a_1$ orbital of pyrimidine, with $E_0 = 250$ eV and $E_b = 20$ eV. The scattered electron detection angles and corresponding momentum transfers are (a) -5°, $|K| = 0.47$ a.u., (b) -10°, $|K| = 0.78$ a.u., and (c) -15°, $|K| = 1.12$ a.u. Points are the experimental data. Solid curve (red): M3DW calculation. Dashed curve (green): M3DW calculation taking the average of the absolute value of the Dyson wave function. The positions of the momentum transfer vector, **K**, and $-$**K** are indicated by the arrows.

Again absolute values are assigned to the experimental data by normalization of the data set to the corresponding M3DW calculation to achieve the best visual fit. For the smallest scattering angle of -5°, the binary peak is somewhat broader than in Fig. 2. As the momentum transfer is increased with increasing scattered electron angle, the binary peak is seen to become narrower. This observation is supported by our M3DW results. All the TDCSs for the $10a_1$ orbital indicate a single binary peak consistent with it being an *s*-type orbital, a result consistent with the classification given in Table I. The EMS study by Ning *et al.*, however, observed a *p*-type momentum distribution at this binding energy.[20] This is likely to be caused by contributions from the $1b_1$ and $6b_2$ orbitals as with the coincidence energy resolution of their apparatus they were unable to separate contributions from these orbitals. While this is also true in our case, it appears from Fig. 3 that with the present kinematics the contribution from the $1b_1$ and $6b_2$ orbitals to the $10a_1$ TDCS is not so severe. Once more it appears that there is very little interaction of the ejected electron with the molecular ion as the $10a_1$ recoil peaks are small in magnitude.

Contrary to the case for the $7b_2$ orbital, where the absolute value of the Dyson wave function is averaged (as taking the average of the molecular wave function would be zero for this symmetry), the totally symmetric nature of the $10a_1$ orbital allows its wave function to be averaged over all orientations. The two types of calculations are compared in Figure 3(c), the method averaging the wave function clearly giving a superior result to the method averaging the absolute value of the wave function. Note that to facilitate comparison, the calculation where the absolute value of the wave function is averaged has been normalized to the calculation averaging the wave function at the maximum of the binary peak. For the scattering angles of -10° and -15° very good qualitative agreement is seen between the M3DW theory and the experimental data. The calculations predict both the shape of the binary peak and the ratio of the binary to recoil peaks very well. Note also that Coulomb repulsion between the final state electrons causes a slight shift of the binary peak, to larger scattering angles, away from the momentum transfer direction.

Agreement between the M3DW calculation and experimental data is not quite as good at the scattering angle of -5°, with the M3DW somewhat underestimating the width of the binary peak. It is possible that this extra width in the experimental cross section is due to contributions from the other unresolved $1b_1$ and $6b_2$ orbitals that are likely to be present. Although the magnitude of the calculated recoil peak is larger than for -10° and -15°, it is still not as large as that observed in the experimental data. As discussed in a previous paper,[17] a similar situation for DWBA type calculations was also observed for tetrahydrofuran and methane[44] for larger impact parameter collisions. Toth and Nagy showed that the magnitude of the recoil peak is related to the nuclear term in the static potential[44] and an underestimation of the recoil peak was attributed to a spreading of the nuclear charge over a spherical shell leading to a nuclear interaction that is too weak.

While good qualitative agreement is observed between the M3DW calculation and experimental data, absolute cross section measurements are needed to assess how close the magnitudes of the predicted TDCSs are to the true values. Unfortunately, placing TDCS data on an absolute scale has traditionally been a difficult process.[45,46] A simple method for absolute (e, 2e) measurements was recently reported,[46] however due to the high density of molecular orbitals such measurements would still be very difficult to perform for a molecular target of the complexity of pyrimidine.

V. CONCLUSIONS

Experimental and theoretical dynamical (e, 2e) results were presented for the pyrimidine molecule, which is a model compound to investigate electron interactions with the DNA bases thymine and cytosine and the RNA base uracil. The measured binding energies and orbital assignments were found to be in good agreement with the available EMS and PES data. Experimental TDCSs for both orbitals investigated exhibited a narrow binary peak at all scattered electron angles with the exception of -5° for the $10a_1$ orbital. The experimental data were also compared with results from theoretical cross sections obtained using the M3DW method. The M3DW calculations taking an average of the molecular wave function gave much better agreement with the experimental data than when the average of the absolute value of the wave function was employed in the calculation. The M3DW calculation predicted a narrower binary peak in the TDCS for the scattering angle of -5° for the $10a_1$ orbital, than is observed in the experimental data. This is likely due to contributions from the $1b_1$ and $6b_2$ orbitals to the experimental data. However, overall we conclude that the M3DW calculations are in rather good qualitative agreement with the experimental data especially given the complicated nature of the molecular target. The good agreement between experiment and theory strongly supports the use of M3DW calculations as input in charged-particle track structure modelling.

ACKNOWLEDGMENTS

This work was supported by the Australian Research Council Centre of Excellence for Antimatter-Matter Studies and by the U.S. National Science Foundation (NSF) (Grant No. PHY-1068237). The author C.N. would like to acknowledge the support of the National Natural Science Foundation of China (NNSFC) (Contract No. 10704046).

[1] B. Boudaïffa, P. Cloutier, D. Hunting, M. A. Huels, and L. Sanche, Science **287**(5458), 1658 (2000).
[2] F. Martin, P. D. Burrow, Z. Cai, P. Cloutier, D. Hunting, and L. Sanche, Phys. Rev. Lett. **93**(6), 068101 (2004).
[3] M. Fuss, A. Munoz, J. C. Oller, F. Blanco, P. Limao-Vieira, C. Huerga, M. Tellez, M. J. Hubin-Fraskin, K. Nixon, M. Brunger, and G. Garcia, in *XXVI International Conference on Photonic, Electronic and Atomic Collisions*, edited by A. E. Orel, A. F. Starace, D. Nikolic, N. Berrah, T. W. Gorczyca, E. Y. Kamber, and J. A. Tanis (IOP, Bristol, 2009), Vol. 194, p. 012028.
[4] D. T. Goodhead, Int. J. Radiat. Biol. **65**(1), 7 (1994).
[5] H. Nikjoo, S. Uehara, D. Emfietzoglou, and F. A. Cucinotta, Radiat. Meas. **41**(9-10), 1052 (2006).
[6] A. Munoz, F. Blanco, G. Garcia, P. A. Thorn, M. J. Brunger, J. P. Sullivan, and S. J. Buckman, Int. J. Mass. Spectrom. **277**(1-3), 175 (2008).

[7]A. Zecca, L. Chiari, G. Garcia, F. Blanco, E. Trainotti, and M. J. Brunger, J. Phys. B **43**(21), 215204 (2010).
[8]J. B. Maljković, A. R. Milosavljević, F. Blanco, D. Šević, G. García, and B. P. Marinković, Phys. Rev. A **79**(5), 052706 (2009).
[9]P. Palihawadana, J. P. Sullivan, M. J. Brunger, C. Winstead, V. McKoy, G. Garcia, F. Blanco, and S. J. Buckman, Phys. Rev. A **84**(6), 062702 (2011).
[10]A. Lahmam-Bennani, J. Phys. B **24**(10), 2401 (1991).
[11]S. Ptasinska, S. Denifl, P. Scheier, and T. D. Mark, J. Chem. Phys. **120**(18), 8505 (2004).
[12]P. Swiderek, Angew. Chem., Int. Ed. **45**(25), 4056 (2006).
[13]R. D. White and R. E. Robson, Phys. Rev. Lett. **102**(23), 230602 (2009).
[14]A. Lahmam-Bennani, A. Naja, E. M. S. Casagrande, N. Okumus, C. Dal Cappello, I. Charpentier, and S. Houamer, J. Phys. B **42**(16), 165201 (2009).
[15]K. L. Nixon, A. J. Murray, H. Chaluvadi, C. Ning, and D. H. Madison, J. Chem. Phys. **134**(17), 174304 (2011).
[16]C. J. Colyer, M. A. Stevenson, O. Al-Hagan, D. H. Madison, C. G. Ning, and B. Lohmann, J. Phys. B **42**(23), 235207 (2009).
[17]C. J. Colyer, S. M. Bellm, B. Lohmann, G. F. Hanne, O. Al-Hagan, D. H. Madison, and C. G. Ning, J. Chem. Phys. **133**(12), 124302 (2010).
[18]C. Dal Cappello, Z. Rezkallah, S. Houamer, I. Charpentier, P. A. Hervieux, M. F. Ruiz-Lopez, R. Dey, and A. C. Roy, Phys. Rev. A **84**(3), 032711 (2011).
[19]D. H. Madison and O. Al-Hagan, Journal of Atomic, Molecular, and Optical Physics **2010**, 367180 (2010).
[20]C. G. Ning, K. Liu, Z. H. Luo, S. F. Zhang, and J. K. Deng, Chem. Phys. Lett. **476**(4-6), 157 (2009).
[21]S. H. R. Shojaei, B. Hajgato, and M. S. Deleuze, Chem. Phys. Lett. **498** (1-3), 45 (2010).
[22]P. O'Keeffe, P. Bolognesi, A. R. Casavola, D. Catone, N. Zema, S. Turchini, and L. Avaldi, Mol. Phys. **107**(19), 2025 (2009).
[23]S. J. Cavanagh and B. Lohmann, J. Phys. B **32**(12), L261 (1999).
[24]E. Weigold and I. E. McCarthy, *Electron Momentum Spectroscopy* (Kluwer Academic/Plenum, New York, 1999).
[25]J. F. Gao, D. H. Madison, and J. L. Peacher, J. Chem. Phys. **123**(20), 204314 (2005).
[26]J. F. Gao, D. H. Madison, and J. L. Peacher, Phys. Rev. A **72**(3), 032721 (2005).
[27]J. F. Gao, J. L. Peacher, and D. H. Madison, J. Chem. Phys. **123**(20), 204302 (2005).
[28]C. Lee, W. Yang, and R. G. Parr, Phys. Rev. B **37**(2), 785 (1988).
[29]C. F. Guerra, J. G. Snijders, G. te Velde, and E. J. Baerends, Theor. Chem. Acc. **99**, 391 (1998).
[30]S. J. Ward and J. H. Macek, Phys. Rev. A **49**(2), 1049 (1994).
[31]J. B. Furness and I. E. McCarthy, J. Phys. B **6**(11), 2280 (1973).
[32]J. P. Perdew and A. Zunger, Phys. Rev. B **23**(10), 5048 (1981).
[33]N. T. Padial and D. W. Norcross, Phys. Rev. A **29**(4), 1742 (1984).
[34]A. W. Potts, D. M. P. Holland, A. B. Trofimov, J. Schirmer, L. Karlsson, and K. Siegbahn, J. Phys. B **36**(14), 3129 (2003).
[35]M. N. Piancastelli, P. R. Keller, J. W. Taylor, F. A. Grimm, and T. A. Carlson, J. Am. Chem. Soc. **105**(13), 4235 (1983).
[36]W. von Niessen, W. P. Kraemer, and G. H. F. Diercksen, Chem. Phys. **41**(1-2), 113 (1979).
[37]R. Gleiter, E. Heilbronner, and V. Hornung, Helv. Chim. Acta **55**(1), 255 (1972).
[38]L. Asbrink, C. Fridh, B. O. Jonsson, and E. Lindholm, Int. J. Mass Spectrom. Ion Phys. **8**(3), 215 (1972).
[39]D. M. P. Holland, A. W. Potts, L. Karlsson, M. Stener, and P. Decleva, Chem. Phys. **390**(1), 25 (2011).
[40]M. Stener, P. Decleva, D. M. P. Holland, and D. A. Shaw, J. Phys. B **44**(7), 075203 (2011).
[41]A. Lahmam-Bennani, H. F. Wellenstein, A. Duguet, and M. Rouault, J. Phys. B **16**(1), 121 (1983).
[42]D. S. Milne-Brownlie, S. J. Cavanagh, B. Lohmann, C. Champion, P. A. Hervieux, and J. Hanssen, Phys. Rev. A **69**(3), 032701 (2004).
[43]A. Naja, E. M. Staicu-Casagrande, A. Lahmam-Bennani, M. Nekkab, F. Mezdari, B. Joulakian, O. Chuluunbaatar, and D. H. Madison, J. Phys. B **40**(18), 3775 (2007).
[44]I. Tóth and L. Nagy, J. Phys. B **43**(13), 135204 (2010).
[45]A. Lahmam-Bennani, M. Cherid, and A. Duguet, J. Phys. B **20**(11), 2531 (1987).
[46]L. R. Hargreaves, M. A. Stevenson, and B. Lohmann, Meas. Sci. Technol. **21**(5), 055112 (2010).